1

Research Developments on Lithium-Ion Batteries

Lishan Yang, Da Xiong, Yangfan Li, Xiang Wang, Boyao Gan, and Xinkang Li

National and Local Joint Engineering Laboratory for New Petrochemical Materials and Fine Utilization of Resources, Hunan Normal University, Changsha 410081, PR China

Outline

The endurance of electric vehicles and the energy storage capacity of power grids demand higher performance from energy storage devices. Since their commercialization in 1991 by Sony, LIBs have rapidly gained traction in both industry and scientific research due to their high output voltage, high energy density [1], and long cycle stability [2, 3]. LIBs are primarily composed of cathode materials [4], anode materials [5], separators, and electrolytes [6]. Over the past three decades, the energy density of LIBs has increased nearly fourfold, solidifying their role in modern technology. The 2019 Nobel Prize in Chemistry was awarded to three pioneering scientists in LIBs research, underscoring their significant contributions to technological advancement [7].

The United States initially led the development of LIBs, followed by Japan and South Korea. Although China entered the LIB industry later, it surpassed Japan and South Korea in lithium-ion car battery patents by 2023 [8, 9]. The LIBs industry value chain includes raw materials, intermediate products, batteries, system integration, and battery recycling, with varying profit margins and revenues across these segments. Battery and new energy vehicle manufacturers dominate the supply chain, but raw material prices significantly impact battery costs. The trend toward vertical integration in the LIBs industry blurs traditional boundaries between upstream, midstream, and downstream sectors, with companies increasingly diversifying their operations.

Declining raw material costs (e.g., lithium carbonate) further enhance LIBs affordability, positioning them for steady growth until 2030. [10].

1.1 Polyanion Cathodes

Polyanion-type cathodes offer several advantages, including low cost, high specific capacity, excellent cycle performance, and enhanced safety [11]. Currently, the main

Electrode Materials in Energy Storage Technologies: Applications in Lithium-, Sodium-, Potassium-, Sulfur- and Zinc-Based Rechargeable Batteries, First Edition. Edited by Liqiang Xu.

Table 1.1 $LiFePO_4$ and $LiFe_{1-X}Mn_XPO_4$ cathode materials production information.

Cathodes	Synthetic technologies	Major producers
$LiFePO_4$	Spray-drying method Solid-phase method Hydrothermal method	Hunan Yuneng New Energy Battery Material, Dynanonic, Fulin Precision Machining
$LiFe_{1-X}Mn_XPO_4$	Spray-drying method Solid-phase synthesis	Ronbay Technology, Lithitech, HCM

commercial polyanion-type cathode materials include $LiFePO_4$ and $LiFe_{1-X}Mn_XPO_4$. Common production methods and manufacturers are summarized in Table 1.1.

1.1.1 Lithium Iron Phosphate

In 1997, Goodenough and colleagues first proposed that $LiFePO_4$ could be used as a cathode material for LIBs [12], has a theoretical specific capacity of 170 mAh g^{-1}. During the charge–discharge process, $LiFePO_4$ and $FePO_4$ are mutually converted. The structure is shown in Figure 1.1a. $LiFePO_4$ belongs to the orthorhombic crystal system and is classified in the Pnma space group. The oxygen atoms create a hexagonal structure, with lithium and iron atoms situated at the center, forming regular FeO_6 and LiO_6 octahedra. A strong covalent bond is formed between P and O, which stabilizes the oxygen atom and prevents its release due to oxidation during charging. The de/intercalation of Li^+ during cycling does not cause a significant change in the volume of $LiFePO_4$, which gives $LiFePO_4$ material strong thermodynamic stability. The P-O tetrahedral structure, interspersed within the Fe-O framework, impedes the deintercalation and intercalation of Li^+ ions during the cycling process. This leads to a low Li^+ diffusion rate and reduced electronic conductivity in $LiFePO_4$ batteries [13]. Under low-temperature conditions, the Li^+ diffusion rate of the material will be further reduced, the charge transfer impedance will be significantly increased, and the battery capacity will be significantly attenuated.

In view of the above problems of $LiFePO_4$, the modification methods are mainly carried out in three aspects [14]: (i) Surface coating: The conductivity between $LiFePO_4$ particles was improved by constructing a stable C coating layer. The conductive coating formed on the surface of the material can effectively control the size of secondary particles, reduce the transmission distance of Li^+ in the material, and improve electrochemical performance. (ii) Ion doping: There are three types of doping: lithium-site doping, iron-site doping, and lithium-iron mixed doping. The ion radius of lithium-site doping is small, such as Mg, Al, and Na. The iron-site-doped ions are mainly Mg, Cu, V and Ti. The doping and function of each site are detailed in Table 1.2. (iii) Morphology control: Nanocrystallization can effectively improve the diffusion rate of Li^+. The preferred crystal orientation was optimized, and the crystal structure of $LiFePO_4$ was changed.

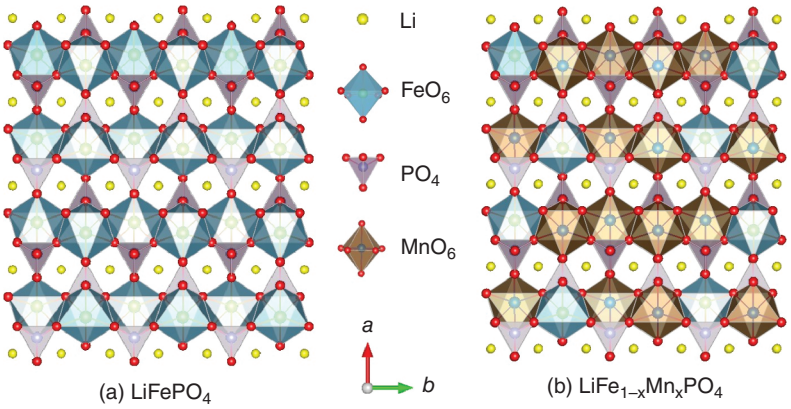

Figure 1.1 The crystal structure simulations of (a) $LiFePO_4$ and (b) $LiFe_{1-X}Mn_XPO_4$.

Table 1.2 The functions of elemental doping on $LiFePO_4$.

Doping sites	Elements	The effects of elemental doping
Li	Mg	Promotes the migration of Li^+
	Ti	Improves conductivity and enhances rate ability
Fe	Cu, V, Ti	Enhances rate ability
	Zn	Increases the transmission space for Li^+ and enhances rate ability
Li and Fe	La, Mg	Improve low-temperature performance
	Mo	Improve conductivity and enhance rate ability

Source: [11]. Electrochemical Energy Reviews 2021/John Wiley & Sons.

1.1.2 Lithium Manganese Iron Phosphate

The structure of $LiFe_{1-X}Mn_XPO_4$ is analogous to that of $LiFePO_4$, as illustrated in Figure 1.1b. $LiFe_{1-X}Mn_XPO_4$ features a voltage platform of 4.1 V for Mn^{2+}/Mn^{3+} and a voltage platform of 3.4 V for Fe^{2+}/Fe^{3+}; the solid solution of iron phosphate and manganese phosphate is formed when all lithium ions are removed [15, 16]. The addition of Mn atoms not only enhances the performance of $LiFePO_4$ materials but also brings new challenges. The difference in the proportion of manganese and iron introduced in the material will significantly cause differences in electrochemical performance: When the content of manganese is too low, the platform voltage is not significantly increased, and the energy density of the material is not significantly increased. When the manganese content is excessively high, it can induce the Jahn–Teller effect, causing lattice distortion. The dissolution of manganese reacts with the electrolyte, which negatively impacts the cycle stability and capacity retention rate [17–19]. The modification is carried out from three aspects [20]: ion doping, surface coating, and morphology control to improve the intrinsic conductivity, rate

Table 1.3 The performance of various $LiFe_{1-X}Mn_XPO_4$ cathode materials.

Cathode materials	Potential window/ V (vs. Li^+/Li)	Discharge capacity at 0.1C (mAh g^{-1})
$LiFe_{0.5}Mn_{0.5}PO_4$	2.7–4.5	142 (0.05C)
$LiFe_{0.6}Mn_{0.4}PO_4$	2.0–4.5	160.2
$LiFe_{0.7}Mn_{0.3}PO_4$	2.5–4.5	162
$LiFe_{0.9}Mn_{0.1}PO_4$	2.5–4.6	145

Source: [21]/John Wiley & Sons.

performance, and phase transition mechanism. The performance of $LiFe_{1-X}Mn_XPO_4$ with common ratios is shown in Table 1.3.

With the rapid growth of the new energy automotive industry and the demand for base station energy storage, significant progress has been made, and the demand for low-cost, high-performance cathodes will continue to rise. Lithium iron phosphate will continue to dominate, and lithium manganese iron phosphate is expected to be more widely used in high-energy-density batteries.

1.2 Layered Oxide Cathodes

Layered oxide cathode materials are pivotal in LIBs due to their high energy density and excellent electrochemical performance [22]. Generally, layered oxide cathode materials include the earliest commercialized lithium cobalt oxide ($LiCoO_2$), high-energy-density nickel cobalt manganese oxides ($LiNi_{1-x-y}Co_xMnyO_2$, NCM), and the current research focus, lithium-rich phase materials ($xLi_2MnO_3 \cdot yLiTMO_2$, LRM). Common production processes and manufacturers and 2023 annual production are listed in Table 1.4.

Discovered by Professor J.B. Goodenough in 1980, $LiCoO_2$ has a theoretical capacity of 274 mAh g^{-1} and remains a primary cathode material for portable electronics [23]. $LiCoO_2$ features an α-$NaFeO_2$-type layered structure, belonging to the hexagonal crystal system, the R-3M space group. The thermodynamically stable O3 phase of $LiCoO_2$ consists of edge-sharing LiO_6 and CoO_6 octahedra. As Li^+ is extracted, the O3 phase undergoes three phase transitions: the first transition occurs at a Li^+ extraction level of 0.07–0.25, resulting in an H1–H2 transition; the second transition occurs at about 0.5 extraction, involving a disordered-to-ordered transition of Li^+ and a structural change from hexagonal to monoclinic; and the third transition occurs at 0.6–0.9 extraction, with the voltage rising to about 4.5 V, resulting in an O3–O1 transition, with the intermediate H1-3 phase causing significant lattice (*c*-axis) and volume contraction. Higher voltages can extract more lithium ions, releasing more energy, but high-voltage charging may lead to rapid capacity, efficiency, and cycle life decay due to surface degradation, destructive phase transitions, and uneven reactions [24]. Doping and surface coating methods are widely used

Table 1.4 Production informations of layered oxide cathode materials.

Cathodes	Synthesis technologies	Producers
$LiCoO_2$	Solid-phase synthesis	RiseSun MGL,
	Coprecipitation method	BSBM,
	Sol–gel method	Ronbay Tech., Xiamen Tungsten
NCM	Coprecipitation method	Ronbay Tech.,
	Solid-phase synthesis	Tianjin B&M, Minmetals New Energy, LG Chem
LRM	Coprecipitation method	Easpring,
	Solid-phase synthesis	Ronbay Tech., BASF Shanshan, Ningxia Hanyao

for material modification. Coating materials include $LiAlO_2$, Al_2O_3, and lithium-ion conductors like Li_2ZrO_3; doping elements include Zr, Al, Ti, Nb, and multielement co-doping [25].

For example, for $LiCoO_2$ materials, the theoretical capacity calculation formula is as follows:

$$C = \frac{n\mathrm{F}}{\mathrm{M}} \tag{1.1}$$

C is the theoretical capacity in mAh g^{-1}, n is the number of moles of electrons transferred per mole of silicon (for $LiCoO_2$, $n = 1$), F is the Faraday constant (96 485 C mol^{-1}), and M is the molar mass of silicon (98 g mol^{-1}). For $LiCoO_2$, this results in a theoretical capacity of approximately 274 mAh g^{-1} [26].

Ternary materials (NCM) partially replace Co in $LiCoO_2$ with Ni and Mn to reduce costs and improve electrochemical performance through synergistic effects among the elements [27]. Different transition metals have unique physical properties: Ni increases cathode capacity, Co enhances charge–discharge kinetics, and Mn improves structural stability during cycling. Various NCM cathode materials are derived based on the ratio of Ni, Co, and Mn, such as 424, 333, 523, and 811. $LiNi_{1-x-y}Co_xMnyO_2$ also has an α-$NaFeO_2$-type layered structure (R-3m space group), with its crystal structure shown in Figure 1.2. Li^+ and transition metals alternately occupy the 3a (0 0 0) and 3b (1 1 1/2) sites, with O^{2-} located at the 6c (0 0 z) site.

In industrial production, the coprecipitation method is the standard synthesis method for polycrystalline ternary cathode materials. Increasing the synthesis temperature promotes grain growth, resulting in single-crystal particles with better stability and electrochemical performance. The theoretical specific capacity of ternary materials is about 275 mAh g^{-1}. Different compositions of ternary materials have different discharge-specific capacities in the voltage range of 2.7–4.3 V, usually

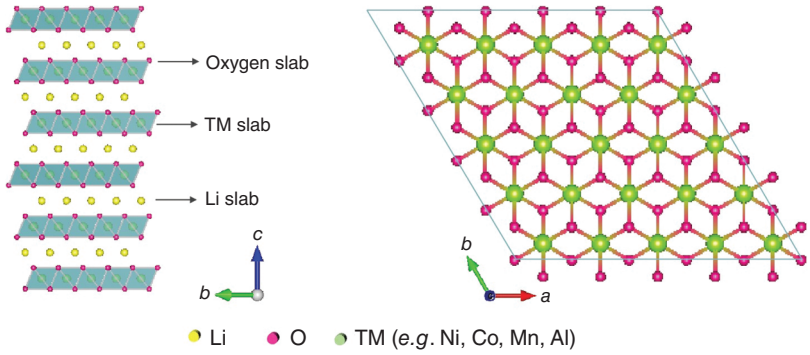

Figure 1.2 The crystal structure simulation of $LiNi_{1-x-y}Co_xMn_yO_2$.

increasing with higher Ni content. As the demand for longer driving ranges and lower battery costs in the electric vehicle market increases, the Ni content in ternary materials continuously increases, making nickel-rich ternary materials an important development direction [28]. However, in ternary LIBs, the cathode material undergoes phase transitions from the original hexagonal phase (H1) to two other hexagonal phases (H2 and H3) during lithium-ion extraction. The failure modes of ternary LIBs are complex behaviors: (i) Due to the similar ionic radii of Ni^{2+} (0.69 Å) and Li^+ (0.76 Å) and their low migration barriers, increasing the Ni content in the material leads to Li–Ni site exchange at the 3b lattice sites, resulting in Li^+/Ni^{2+} cation mixing. This cation mixing obstructs the Li^+ transport channels, leading to low initial efficiency and poor long-term cycling performance of the battery [29]. (ii) The extraction of Li^+ ions necessitates charge compensation, resulting in the formation of highly oxidative Ni^{4+} species. These species facilitate the decomposition of the electrolyte on the cathode surface, consuming active lithium ions in the system and compromising the thermal stability of the material [30]. (iii) H^+ species in the electrolyte attack the surface of the cathode material, causing the dissolution of transition metal ions from the electrode surface. This induces heterogeneous interfacial chemical reactions, increasing interfacial impedance. Additionally, the dissolved transition metal ions may migrate to the anode surface and deposit on the solid electrolyte interphase (SEI) layers [31]. To address these issues, ion doping, morphology control, and concentration gradient methods are employed to enhance the electrochemical performance of ternary materials [32, 33]. Table 1.5 lists the effects of different element doping, and Table 1.6 shows the types and main functions of commonly used coating materials.

When the Co position in the layered structure also contains Li, the material is referred to as lithium-rich cathode material $xLi_2MO_3 \cdot (1-x)LiM_2$ (M = Ni, Co, Mn). This material typically consists of a composite of Li_2MnO_3 and $LiMO_2$-layered structures in varying proportions, with a theoretical capacity of up to 280 mAh g^{-1}. $LiMO_2$ belongs to the hexagonal crystal system with the same α-$NaFeO_2$ configuration (R-3m space group) as $LiCoO_2$, while Li_2MnO_3 has a superstructure ordering of Li and Mn atoms, belonging to the monoclinic crystal system.

Table 1.5 The effects of elemental doping on NCM cathodes.

Elements	Main effects
Mg	Cation ordering and "pillar" effect
Al	Relieving phase transition and refining particles
Zr	Cation ordering and "pillar" effect
Ti	Cation ordering and "pillar" effect
B	Modulating microstructure
W	Decreasing the surface passivation layer
Na	Improving Li^+ kinetics and mitigating transition metals migration
K	Improving Li^+ kinetics and mitigating transition metals migration
F	Enhancing the oxygen framework stability
S	Enhancing the oxygen framework stability
Nb	Spheroidization of primary particles

Source: [32]/John Wiley & Sons.

Table 1.6 Various coating materials and main effects.

Coating layers		Main effects
Metal oxides	Al_2O_3 TiO_2 CeO_2	Initiative coating protective layers
Phosphates	$AlPO_4$ $Cu_3(PO_4)_2$	Improvement of cyclic and thermal stability
Fluorides	AlF_3 LiF	Prevention of corrosion by hydrofluoric acid
Lithium transition metal oxides	Li_2ZrO_3 $Li_4Ti_5O_{12}$ $LiAlO_2$ $Li_{1.3}Al_{0.3}Ti_{1.7}(PO_4)_3$	Protective layer with excellent lithium-ion conductivity
Carbon materials	PPy CNT	Improvement of structural stability and electronic/Li^+ conductivity

Source: [33]. Oxygen loss in layered oxide cathodes/John Wiley & Sons.

Lithium-rich phase materials have a high lithium/transition metal molar ratio and higher discharge capacity. However, during charging, the oxygen anions in lithium-rich phase materials partially oxidize to O^- radicals or oxygen gas and escape from the lattice, reacting with the electrolyte [34]. During cycling, transition metals enter the Li layer, causing the material to transition to a spinel structure, lowering the discharge plateau [35]. Surface modification, bulk doping,

and electrolyte design methods can alleviate lattice oxygen loss and metal ion migration in lithium-rich manganese-based materials during cycling, improving cycle performance and initial coulombic efficiency [36].

1.3 Spinel Structure Cathodes

Lithium manganese oxide ($LiMn_2O_4$) and high-voltage lithium nickel manganese oxide (LNMO) are both spinel-type cathode materials utilized in LIBs [37]. They are characterized by their high energy density, excellent cycle stability, and prolonged service life, rendering them extensively applied within the battery industry [38]. According to the statistics of Huajing Industrial Research Institute, the output of the lithium manganate industry in 2021 has been greatly improved compared with 2020, with an output of 87 400 tons, an increase of 45.9%. The import volume was 305.84 tons. The year-on-year growth was 42.05%, and the export volume was 468.96 tons, a decrease of 8.88%. Common production processes and major manufacturers are delineated in Table 1.7 for reference.

The first lithium manganate cathode material with three-dimensional lithium-ion channels was developed by Hunter in 1981 [39]. In LIBs, charge and discharge with $LiMn_2O_4$ as the cathode are shown as follows:

Cathode:

$$LiMn_2O_4 \underset{\text{discharge}}{\overset{\text{charge}}{\rightleftharpoons}} Li_{1-\lambda}Mn_2O_4 + \lambda Li^+$$

During the charging process, 8a lithium ions traverse the 8a–16c–8a channel to dissociate from the three-dimensional lattice, while Mn^{3+} undergoes electron loss and oxidation to become Mn^{4+}. Upon discharging, lithium ions are incorporated into the 8a position under the influence of electrostatic force, while Mn^{4+} acquires electrons and is reduced to Mn^{3+}, ultimately leading to a structural transformation into $LiMn_2O_4$. Manganese dioxide was regarded as one of the most promising cathode materials for LIBs due to its theoretical specific capacity of 148 mAh g^{-1} and a discharge voltage plateau at 4.15 V. However, the Jahn–Teller effect gives rise to significant capacity degradation issues such as material deterioration and electrolyte

Table 1.7 $LiMn_2O_4$ and $LiNi_{0.5}Mn_{1.5}O_4$ cathode materials production information.

Cathodes	Synthetic technologies	Major producers
$LiMn_2O_4$	Solid-phase synthesis Microwave synthesis Hydrothermal synthesis	DX Energy, Boshi High-Tech., Xiangtan Electrochemical, Xinxiang Hongli, South Manganese
$LiNi_{0.5}Mn_{1.5}O_4$	Solid-phase synthesis	Boshi High-Tech., BSBM

decomposition [40]. The most effective solution to this problem involves partially substituting Mn with other metal ions (such as Li, Mg, Al, Ti, Cr, Ni, and Co) and modifying the surface of the materials [41, 42].

High-pressure lithium nickel manganate $LiNi_{0.5}Mn_{1.5}O_4$ was first reported by Blasse in 1964 as specific $LiNi_{0.5}Mn_{1.5}O_4$ along with a series of mixed metal spinel oxides [43]. Lithium nickel manganate crystals have two different structures: one is a disordered structure, which is also known as the spinel type and expressed as D-LNMO, in which nickel and manganese ions are disordered at the 16d site of the lattice. The other is the olivine structure, represented as O-LNMO, in which nickel and manganese ions are orderly distributed in the lattice, occupying the 4a and 12d sites, respectively. Its reversible capacity is 146.7 mAh g^{-1}, similar to that of lithium manganate; in the battery charging process, lithium ions will be removed from a specific point through a three-dimensional channel; Ni^{2+} and Ni^{3+} will be oxidized into Ni^{4+}; and $LiNi_{0.5}Mn_{1.5}O_4$ will eventually be converted into $Ni_{0.5}Mn_{1.5}O_4$; and the discharge process is opposite to the charging process. The high-voltage lithium nickel manganate discharge voltage can reach 4.7 V, mainly because of its unique chemical composition and electrochemical properties; nickel provides a higher voltage; and manganese helps to inhibit the excessive oxidation of nickel. However, when it is operated under high-voltage conditions during the cycle, side reactions occur between its surface and electrolyte, resulting in a short cycle life due to rapid capacity decline [44]. Doped metal ions and surface coatings can be used to reduce side reactions [45, 46].

Lithium manganate is an important precursor for the synthesis of other LIBs cathode materials, such as lithium-rich materials, multicomponent materials, and solid lithium manganese oxides. Also, the solid-state battery made of high-pressure lithium nickel manganate material as a positive electrode has higher energy density, higher safety, and lower cost advantages than ordinary lithium ions. It is believed that under this development trend, lithium manganate and high-pressure lithium nickel manganate will be more widely used.

1.4 Anode Materials

Anode materials are crucial for the electrochemical performance of LIBs. Pure lithium metal is ideal due to its high capacity and lightweight, but safety concerns with lithium dendrites limit their use. Currently, anode materials are categorized into carbon and non-carbon types. Carbon materials include graphite, soft carbon, and hard carbon. Non-carbon materials encompass silicon-based materials, lithium titanate, and tin-based materials [47–49].

The ideal anode material for LIBs should possess low chemical potential, high coulombic efficiency, and good electrical conductivity, stability, and compatibility; should be abundant; and should have low cost. Currently, graphite carbon is the most widely used anode material, offering the best overall performance to meet these criteria. In battery production, anode materials account for about 10% of the total material cost. Research is focused on developing low-cost, high-capacity

anode materials. Silicon-based materials are promising for next-generation high-energy-density LIBs due to their high theoretical capacity, environmental friendliness, and abundant reserves. The specific details of common lithium anode materials are shown in Table 1.8 [56, 57, 59].

For example, for silicon-based materials, the theoretical capacity calculation formula is as follows:

$$C = \frac{n\mathrm{F}}{\mathrm{M}} \tag{1.2}$$

C is the theoretical capacity in $\mathrm{mAh\,g^{-1}}$, n is the number of moles of electrons transferred per mole of silicon (for silicon, $n = 4.4$), F is the Faraday constant ($96\,485\,\mathrm{C\,mol^{-1}}$), and M is the molar mass of silicon ($28.0855\,\mathrm{g\,mol^{-1}}$). For silicon, this results in a theoretical capacity of approximately $4200\,\mathrm{mAh\,g^{-1}}$ [60].

As new energy vehicles and energy storage markets rapidly develop, the need for high-performance anode materials will continue to increase. While graphite anode materials will remain prevalent, emerging alternatives like silicon-based and SiO_x materials are anticipated to see broader application in high-energy-density batteries. Advancements in technology and process enhancements will be crucial for the progress of anode materials.

1.5 Cell Technology

The cell technology of energy storage batteries refers to the unit technology used to store and release electrical energy in energy storage batteries, mainly involving cell materials and cell integration technology. The cell technology is a key factor in determining the output power density, cost, and service life of energy storage batteries [61, 62].

1.5.1 Battery Cells

With the rapid increase in demand in the energy storage market, various types of energy storage cells have been developed, as shown in Figure 1.3, and have been widely used. Coin cells have the advantages of small size, safe and convenient use, and wide applicability in various electronic products. The full-cell button battery assembled from lithium iron phosphate/graphite and NCM811/silicon can achieve the specific energy of 100–160 and 300–350 $\mathrm{Wh\,kg^{-1}}$ and the specific power of 160–230 and 300–350 $\mathrm{Wh\,kg^{-1}}$, respectively [63]. The specific energy (E) and specific power (P) are calculated as follows:

$$E = \frac{k \cdot \Delta U \cdot C_p}{M} \tag{1.3}$$

k is the mass fraction of the active material, that is, the sum of the cathode active material mass m_p and the anode active material mass m_n divided by the total cell

Table 1.8 Main parameters of various anode materials for lithium-ion batteries.

Anode	Lithium storage mechanism	Storage potential/V (vs. Li^+/Li)	Specific capacity/(mAh g^{-1})	Initial coulombic efficiency/%	Major producers	Ref.
Graphite	Intercalation mechanism	~ 0.1	372	85–90	BTR, BSBM, etc.	[50]
Hard carbon	Adsorption–intercalation mechanism, intercalation–adsorption mechanism, adsorption–intercalation–adsorption mechanism, etc.	0–1.5	200–600	~ 70	Kureha Corporation, SGL Carbon, etc.	[51–53]
Soft carbon	Adsorption–intercalation mechanism, etc.	0–1.2	> 350	~ 50	BSBM, BTR, etc.	[54]
Si	Alloying reaction mechanism	< 0.1	650–4200	65–93	Shin-Etsu Chemical Co., Ltd., SUMCO Corporation, etc.	[55]
Si/C composite anode	Alloying reaction and intercalation mechanism	0.01–1.5	700–3500	47–95	Group14 Technologies, Showa Denko, etc.	[56, 57]
SiO_x	Conversion reaction and alloying reaction mechanism	0.01–0.5	785–2875.2	44–82.2	Mitsubishi Chemical, Toppan Printing, etc.	[58]

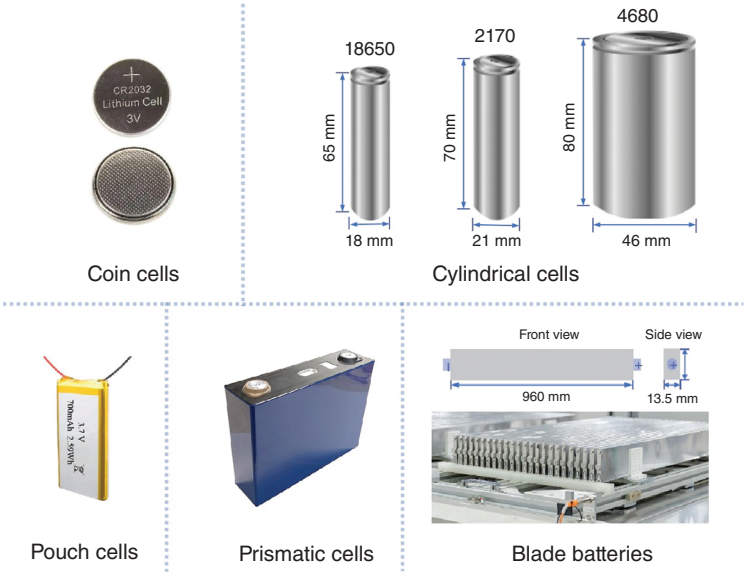

Figure 1.3 The pictures of commercial coin cells, cylindrical cells, pouch cells, prismatic cells, and blade batteries.

mass. ΔU is the average voltage difference between the cathode and anode. C_p is the gram capacity of the cathode active material. M is the total battery mass.

$$P = \frac{E}{\sqrt{t}} \tag{1.4}$$

E is the specific energy. t is the discharge time.

Additionally, the cylindrical cells have the characteristics of large capacity, long cycle life, and wide operating ambient temperature, which have gained a firm foothold in the power market with the unified model and standardized production. Japan's Sony company first designed a standard LIB, the 18 650 cylindrical cells (18 mm diameter and 65 mm axial length) [64], but the energy density is lesser and the charging speed is slower. Compared to the 18 650 battery, the energy density of the whole package composed of the 2170 battery (21 mm diameter and 70 mm axial length) can be further improved, and the charging speed can be faster. Later, Tesla's 4680 battery (46 mm diameter and 80 mm axial length) only changed in terms of cell design, while the levelized cost of electricity (LCOE) of the cell was reduced by about 14% compared with the 2170 battery, and the power of a single cell was increased to 5.48 times. Many other battery types, such as pouch cells, have the advantage of high energy density and lightweight but require additional protection against battery damage and thermal runaway. Prismatic cells are currently the most widely used cells in the international field, which have advantages such as high strength, small internal resistance, and high space utilization; however, it is difficult to unify the standard production process, and the heat dissipation during operation is poor.

The blade battery is a single battery with a long and thin blade-like shape and adopts cell-to-pack (CTP) module-free integration technology [64]. The cell structure adopts the design of the battery pack instead of the traditional shell structure; meanwhile, the beam and cell of the battery are directly applied by the blade battery; and finally, the top and bottom are connected by aluminum plates.

BYD launched the lithium iron phosphate blade batteries in 2020, which increase the energy density by 50%, reduce the manufacturing cost by 30% without changing the battery system, and can withstand safety level tests such as collision, high temperature, and puncture, which greatly expands the application field of LIBs.

The blade battery is a single battery with a long and thin blade-like shape and adopts CTP module-free integration technology. Due to the change in the battery structure, the design of the battery pack cancels the shell structure of the traditional battery. The blade battery acts as the beam and cell of the battery and then adopts the design of honeycomb aluminum plates, with two high-strength aluminum plates pasted on the upper and lower sides. The blade batteries are arranged within this structure.

1.5.2 Cell Integration Technology

In the early days, major battery manufacturers mainly used cell-to-module (CTM) cell integration [65], which is a mode that integrates battery cells directly into modules, and the general configuration method is "cell–module–pack loading," but the space utilization rate of the module configuration mode is only 40%, and with the increase of energy density requirements of power trams, it is gradually replaced by technologies such as CTP and cell to chassis (CTC). CTP integration technology integrates the battery cells directly into the battery pack, eliminating the need for standardized module linking, also known as "module-less battery" [66]. From the perspective of product performance, compared to conventional battery packs, the CTP method has increased the volume utilization rate by 15–20% and the production efficiency by 50%, and the energy density can reach more than 200 Wh/kg, while effectively reducing costs. As a result, CTP has become a mainstream battery cell integration technology [67]. Products with typical CTP technology include BYD's blade batteries, CATL's Kirin batteries, and Svolt Energy Technology Co., Ltd. (SVOLT's) short-knife batteries. The CTC first proposed by Tesla is considered to be the key core technology in the next stage of new energy vehicles. CTC technology directly integrates the battery cell into the vehicle chassis [68]. It reduces the loss of space caused by the connection between the car body and the battery cover, thus improving space utilization.

1.6 Electrolyte

The electrolyte is a vital component in every electrochemical device [69], which plays a pivotal role in promoting the migration of ions between the anode and cathode, and is vividly called the "blood" of the battery. The electrolyte not only

plays an important role in regulating the performance of the electrode and the electrolyte interface but also directly impacts the specific capacity, internal resistance, charge and discharge performance rates, operating temperature range, and storage characteristics of the battery [68]. To date, the mainstream LIBs electrolytes are often composed of solvents, lithium salts, and functional additives.

The primary constituent of the electrolyte is an organic solvent, which can dissolve lithium salts and deliver a carrier for lithium ions. An ideal LIBs electrolyte requires organic solvents to meet a variety of conditions [70]: high dielectric constant to ensure sufficient dissolution of lithium salts; low viscosity; high electrochemical and chemical stability; low melting point, high boiling point, and high flash point; and non-toxic, harmless, and cost-effective. Currently, the commonly used organic solvents are mainly carbonates and organic ethers, as shown in Table 1.9. In addition, a single solvent is difficult to meet the requirements of batteries in extreme environments, so mixed solvents are often used to combine multiple excellent properties.

The application of lithium salt in LIBs needs to meet the following characteristics [71]: high solubility in organic solvents, easy dissociation to release Li^+ ions, and high conductivity. It exhibits excellent antioxidant stability and remains unaffected by electrochemical and thermodynamic reactions with organic solvents, electrode materials, and battery components. Moreover, it is environmentally friendly and boasts straightforward preparation, purification, and industrial scalability. Commonly used lithium salts are shown in Table 1.10.

Electrolyte additives refer to specific chemicals mixed into the electrolyte. In general, the number of additives is not more than 20% by weight or volume percentage. Compared with conventional electrolytes, including only solvents and lithium salts, electrolytes containing different additives have a huge impact on battery performance, which can adjust some physical and chemical properties of the battery and significantly enhance the electrochemical performance [73]. The common types of electrolyte addition and their effects are shown in Table 1.11.

Table 1.9 Physical properties of common organic solvents.

Solvents	Dielectric constant	Boiling point /°C	Melting point /°C
Ethylene Carbonate (EC)	89.78	248	36.4
Propylene Carbonate (PC)	64.9	242	−48.8
Dimethyl Carbonate (DMC)	3.11	91	4.6
Diethyl Carbonate (DEC)	2.81	126	−74.3
1,2-Dimethoxyethane (DME)	5.5	82.5	−58
Ethyl Methyl Carbonate (EMC)	2.96	110	−53
Ethyl Acetate (EA)	6.02	77	−84
Tetrahydrofuran (THF)	7.58	66	−108.5
Dipropyleneglycol Dimethyl Ether (DMM)	2.7	41	−105

Source: [71]/John Wiley & Sons.

Table 1.10 Common lithium salts and their advantages and disadvantages.

Salts	Advantages	Disadvantages
$LiPF_6$	Soluble, high ionic conductivity, and capable of forming a stable passivation film on the current collector surface	Poor thermal stability and prone to decomposition reactions
$LiBF_4$	Wide operating temperature range and good stability at high temperatures	Low ionic conductivity
LiBOB	High conductivity, a wide electrochemical window, and excellent thermal stability contribute to the formation of the SEI film	Low solubility
LiDFOB	Good film-forming and low-temperature performance, with higher solubility in carbonate solvents and higher electrolyte conductivity	Expensive
LiTFSI	Enhanced solubility and conductivity, along with a high thermal decomposition temperature and hydrolysis resistance	Corrosive to aluminum foil
LiFSI	High conductivity	Corrosive to aluminum foil
$LiPO_2F_2$	Excellent low- and high-temperature performance	Low solubility

Source: [72]/John Wiley & Sons.

Table 1.11 Common additives and their functions.

Additives	Functions
Fluoroethylene Carbonate (FEC)	SEI-forming additive
Biphenyl	Overcharge protection additive
Triphenyl Phosphate/Tributyl Phosphate	Flame-retardant additive
Graphene	Conductive additive

Source: [73]/John Wiley & Sons.

1.7 Binders

During the assembling of the electrodes, binders are polymer compounds which can adhere the cathode or anode active substances to the current collectors. The binder mainly has the following functions: first, the binder acts as a dispersant or thickening agent to improve the uniformity of electrode components. Second, the binder can bind the conductive agent, active substance, and fluid collector to maintain the integrity of the electrode structure. Finally, the wettability of the electrolyte is improved to promote the conveyance of Li^+ at the electrode–electrolyte interface [74, 75].

The desirable binder should have the following characteristics: (i) the binder should not have an electrochemical reaction with the electrolyte or other substances. (ii) The binder should have good dispersion, and its dispersion effect is related to surface charge density, main-chain flexibility, and electrostatic repulsion effect. (ii) The binder must have excellent mechanical traits, such as elasticity, hardness, and adhesion strength. These properties are related to the molecular weight and functional group of the binder. (iv) The binder also needs to have good electrical conductivity, which can be improved by gas-phase doping, electrochemical doping, solvent doping, and ion-exchange doping. (v) The binder should be able to maintain stability under a certain ambient temperature and humidity to avoid affecting the battery performance due to changes in temperature and humidity [76, 77]. Commonly used binders are listed in Table 1.12. However, there is currently no binder that fully meets all of the above requirements. Therefore, when selecting binders, the selection should be optimized according to the specific application environment and needs. By taking these factors into account, the binder that is most suitable for the specific application can be selected, thereby raising the performance and life of the battery.

With the incessant progress of LIBs technology, more and more new binders have begun to enter people's vision, such as polyimide (PI) [78, 79]. These new binders have significant potential to improve battery performance, extend battery life, and enhance environmental adaptability. In the future, the custom design of binders will become an important direction, and it will be developed according to factors such as the morphology, state, and functional groups of the material surface to satiate the demands of high-energy-density batteries.

1.8 Outlook

In the modern era, information and transportation technologies are increasingly dependent on rechargeable batteries, creating a pressing need for higher energy density. For over 15 years, LIBs have been the primary power source for portable electronic devices, achieving high maturity and reliability. However, the quest for greater energy density remains a focal point for global research communities and intensive industry research and development (R&D) efforts. This necessitates the development of new, advanced rechargeable LIBs and a comprehensive understanding of their working mechanisms during charge and discharge cycles.

Traditional LIBs utilize liquid electrolytes that typically contain highly volatile and flammable organic solvents, which increase the risk of fire and explosion and limit their ability to withstand high operating voltages. Additionally, liquid electrolytes react with lithium metal to form an unstable SEI layer, leading to the growth of harmful lithium dendrites. In contrast, solid-state LIBs employ solid electrolytes, significantly enhancing safety and reducing the risk of fire and explosion. Solid-state batteries offer higher energy density, longer cycle life, and faster charging speeds, thereby improving the user experience. With the development of solid electrolytes such as oxides, sulfides, and polymers, solid-state LIBs have

Table 1.12 Common binders and their advantages and disadvantages.

Types	Applications	Advantages	Disadvantages
Polyvinylidene Fluoride (PVDF)	$LiMO_2$ (M = Co, Ni, Mn, Al), $LiFePO_4$(LFP), $LiMn_2O_4$, $LiMn_xNi_yCo_zO_2$, Si, Sn, TiO_2, SnO_2, $NaMnO_2$, $NaV(PO_4)_2F_3$, MoS_2, MnO_2/MWCNT, MnO_2/graphene, etc.	Good corrosion resistance, good heat resistance, and good processability	Low adhesion strength, high cost, and poor electrical conductivity
Carboxymethyl Cellulose (CMC)	$LiMO_2$, $LiFePO_4$, $LiNi_{0.4}Mn_{1.6}O_4$, $LiMn_2O_4$, Si, $Li_4Ti_5O_{12}$, SnO_2, Sn, TiO_2, LI-S, P, Sb, oxides, $NaMnO_2$, $NaV(PO_4)_2F_3$, PFPT, etc.	High adhesion, can improve battery capacity and cycle life, and has good thermal stability and electrochemical characteristics	Large brittleness, poor elasticity, and easy moisture absorption
Styrene-Butadiene Rubber (SBR)	$LiMO_2$, $LiFePO_4$, TiO_2, Li-S, carbonaceous materials, Si, etc.	The high bonding force	High cost
Sodium Alginate (Alg-Na)	$LiMO_2$, carbonaceous materials, Si, MoS_2, metal oxides, etc.	Environmental protection, low cost, and good adhesion and mechanical properties	Improvements are needed to adapt to different material systems
Polytetrafluoroethylene (PTFE)	Li-O_2, $LiFePO_4$, carbonaceous materials, MnO_2/graphene, PANI/CNT/graphene, etc.	Good corrosion resistance, good heat resistance, and good aging resistance	High cost, high thermal expansion rate, and low mechanical strength
Polyacrylic Acid (PAA)	$LiFePO_4$, $LiMn_2O_4$, carbonaceous materials, Si, Li-S, P, Sn, oxides, etc.	The low expansion coefficient and high thermal diffusion coefficient can ensure the structural integrity of the silicon-based electrode during the cycle	Great brittleness

Source: Refs. [78, 79].

broad application prospects in renewable energy storage, consumer electronics, and electric transportation and are expected to lead a new revolution in battery technology. Although aqueous LIBs currently face the challenge of lower energy density, their safety, low cost, and environmental friendliness make them an emerging research hotspot.

In the exploration of battery working mechanisms, in-situ characterization techniques provide multi-angle real-time data analysis by monitoring operating batteries with high temporal resolution. For example, in-situ X-ray diffraction (XRD), Raman spectroscopy, and scanning transmission electron microscopy (STEM) can be used to observe phase changes and lattice parameters of electrodes or electrode–electrolyte interfaces in real time during charge–discharge cycles, providing critical insights and data support for studying battery working and failure mechanisms. To achieve higher battery energy density, it is essential to promote innovation in cell structure and platformization of battery systems. This involves seeking the optimal cell structure by integrating factors such as lightweight, safety, and rate performance and aligning with typical structures like blade batteries, large cylindrical batteries, and large pouch batteries, while accelerating the standardization of cell sizes.

With the widespread application of computers in materials science, theoretical simulations can help researchers understand the microstructure and electrochemical reaction mechanisms of battery materials, guiding material design and performance optimization. Additionally, artificial intelligence technologies, such as machine learning and deep learning, can be employed for big data analysis and prediction, accelerating the discovery of new materials and optimization of battery performance. Finally, combining theoretical simulations and artificial intelligence methods can enable predictions and management of the entire battery lifecycle, enhancing battery efficiency and lifespan.

References

1 Wang, Q., Lu, T., Xiao, Y. et al. (2023). Leap of Li metal anodes from coin cells to pouch cells: challenges and progress. *Electrochemical Energy Reviews* 6 (1): 22.

2 Manthiram, A. (2020). A reflection on lithium-ion battery cathode chemistry. *Nature Communications* 11 (1): 1550.

3 Liu, T.; Yu, L.; Liu, J. et al. (2024). Ultrastable cathodes enabled by compositional and structural dual-gradient design. *Nature Energy* 9: 1252–1263.

4 Winter, M., Barnett, B., and Xu, K. (2018). Before Li ion batteries. *Chemical Reviews* 118 (23): 11433–11456.

5 Xiao, J., Shi, F., Glossmann, T. et al. (2023). From laboratory innovations to materials manufacturing for lithium-based batteries. *Nature Energy* 8 (4): 329–339.

6 Chen, Y., Qin, Q., Zhao, L. et al. (2024). Analysis of China's patent landscape for new energy storage technologies. *Energy Storage Science and Technology.* 13 (06): 2089–2098.

7 Xie, J. and Lu, Y.-C. (2024). Designing nonflammable liquid electrolytes for safe Li-ion batteries. *Advanced Materials* 2312451.

8 Deng, Z., Chen, S., Yang, K. et al. (2024). Tailoring interfacial structures to regulate carrier transport in solid-state batteries. *Advanced Materials* 2407923.

9 Orangi, S., Manjong, N.B., Clos, D.P. et al. (2023). Trajectories for lithium-ion battery cost production: can metal prices hamper the deployment of lithium-ion batteries. *Batteries & Supercaps* 6 (12): e202300346.

10 Clément, R.J., Lun, Z., and Ceder, G. (2020). Cation-disordered rocksalt transition metal oxides and oxyfluorides for high energy lithium-ion cathodes. *Energy & Environmental Science* 13 (2): 345–373.

11 Liu, Y., Li, W., and Xia, Y.Y. (2021). Recent progress in polyanionic anode materials for Li (Na)-Ion batteries. *Electrochemical Energy Reviews* 4 (3): 447–472.

12 Padhi, A.K., Nanjundaswamy, K.S., and Goodenough, J.B. (1997). Phospho-olivines as positive-electrode materials for rechargeable lithium batteries. *Journal of the Electrochemical Society* 144 (4): 1188.

13 Li, B., Xiao, J., Zhu, X. et al. (2024). Enabling high-performance lithium iron phosphate cathodes through an interconnected carbon network for practical and high-energy lithium-ion batteries. *Journal of Colloid and Interface Science* 653: 942–948.

14 Zhao, T., Mahandra, H., Marthi, R. et al. (2024). An overview on the life cycle of lithium iron phosphate: synthesis, modification, application, and recycling. *Chemical Engineering Journal* 485: 149923.

15 Nekahi, A., MR, A.K., Li, X. et al. (2024). Sustainable $LiFePO_4$ and $LiMn_xFe_{1-x}PO_4$ (x=0.1–1) cathode materials for lithium-ion batteries: A systematic review from mine to chassis. *Materials Science and Engineering: R: Reports* 159: 100797.

16 Manthiram, A. (2020). A reflection on lithium-ion battery cathode chemistry. *Nature Communications* 11 (1): 1550.

17 Deng, Y., Yang, C., Zou, K. et al. (2017). Recent Advances of Mn-Rich $LiFe_{1-y}Mn_yPO_4$ ($0.5 \leq y < 1.0$) Cathode materials for high energy density lithium ion batteries. *Advanced Energy Materials* 7 (13): 1601958.

18 Li, S., Zhang, H., Liu, Y. et al. (2024). Comprehensive understanding of structure transition in $LiMn_yFe_{1-y}PO_4$ during delithiation/lithiation. *Advanced Functional Materials* 34 (4): 2310057.

19 Yang, R., Chang, L., Luo, S. et al. (2024). A critical revelation of lithium ferromanganese phosphate (LMFP) performance in a Mn-rich cathode for Li-ion batteries using Fe equivalents to occupy a Mn site. *Journal of Materials Chemistry C* 12 (14): 4961–4976.

20 Nasajpour-Esfahani, N., Garmestani, H., Bagheritabar, M. et al. (2024). Comprehensive review of lithium-ion battery materials and development challenges. *Renewable and Sustainable Energy Reviews* 203: 114783.

21 Sun, K., Luo, S.-H., Du, N. et al. (2024). Research progress of lithium manganese iron phosphate cathode materials: from preparation to modification. *Electroanalysis* e202400120.

22 Manthiram, A.J.N. (2020). A reflection on lithium-ion battery cathode chemistry. *Nature Communications* 11 (1): 1550.

23 Mizushima, K., Jones, P.C., Wiseman, P.J., and Goodenough, J.B. (1981). Li_xCoO_2 ($0< x\leqslant 1$): A new cathode material for batteries of high energy density. *Solid State* 3: 171–174.

24 Lyu, Y., Wu, X., Wang, K. et al. (2021). An overview on the advances of $LiCoO_2$ cathodes for lithium-ion batteries. *Advanced Energy Materials* 11 (2): 2000982.

25 Konar, R., Maiti, S., Shpigel, N., and Aurbach, D. (2023). Reviewing failure mechanisms and modification strategies in stabilizing high-voltage $LiCoO_2$ cathodes beyond 4.55 V. *Energy Storage Materials* 103001.

26 Lyu, Y.C., Wu, X., Wang, K. et al. (2021). An Overview on the Advances of $LiCoO_2$ Cathodes for Lithium-Ion Batteries. *Advanced Energy Materials* 11 (2).

27 de Biasi, L., Schwarz, B., Brezesinski, T. et al. (2019). Chemical, structural, and electronic aspects of formation and degradation behavior on different length scales of Ni-rich NCM and Li-rich HE-NCM cathode materials in Li-ion batteries. *Advanced Materials* 31 (26): 1900985.

28 Li, W., Erickson, E.M., and Manthiram, A.J.N.E. (2020). High-nickel layered oxide cathodes for lithium-based automotive batteries. *Nature Energy* 5 (1): 26–34.

29 Manthiram, A., Song, B., and Li, W. (2017). A perspective on nickel-rich layered oxide cathodes for lithium-ion batteries. *Energy Storage Materials* 6: 125–139.

30 Sim, R. and Manthiram, A. (2024). Factors influencing gas evolution from high-nickel layered oxide cathodes in lithium-based batteries. *Advanced Energy Materials* 14 (8): 2303985.

31 Deng, Z., Liu, Y., Wang, L. et al. (2023). Challenges of thermal stability of high-energy layered oxide cathode materials for lithium-ion batteries: a review. *Materials Today* 236–261.

32 Liu, C., Cui, Z., and Manthiram, A. (2024). Tuning dopant distribution for stabilizing the surface of high-nickel layered oxide cathodes for lithium-ion batteries. *Advanced Energy Materials* 14 (3): 2302722.

33 Zhang, H., Liu, H., Piper, L.F. et al. (2022). Oxygen loss in layered oxide cathodes for Li-ion batteries: mechanisms, effects, and mitigation. *Chemical Reviews* 122 (6): 5641–5681.

34 Zhao, S., Yan, K., Zhang, J. et al. (2021). Reaction mechanisms of layered lithium-rich cathode materials for high-energy lithium-ion batteries. *Angewandte Chemie International Edition* 60 (5): 2208–2220.

35 Zhao, S., Guo, Z., Yan, K. et al. (2021). Towards high-energy-density lithium-ion batteries: strategies for developing high-capacity lithium-rich cathode materials. *Energy Storage Materials* 34: 716–734.

36 Kim, S., Cho, W., Zhang, X. et al. (2016). A stable lithium-rich surface structure for lithium-rich layered cathode materials. *Nature Communications* 7 (1): 1–8.

37 Li, W., Lee, S., and Manthiram, A. (2020). High-nickel NMA: a cobalt-free alternative to NMC and NCA cathodes for lithium-ion batteries. *Advanced Materials* 32 (33): 2002718.

38 Song, J., Wang, H., Zuo, Y. et al. (2023). Building better full manganese-based cathode materials for next-generation lithium-ion batteries. *Electrochemical Energy Reviews* 6 (1): 20.

39 Hunter, J.C. (1981). Preparation of a new crystal form of manganese dioxide: λ-MnO_2. *Journal of Solid State Chemistry* 39: 142–147.

40 Zuo, C., Hu, Z., Qi, R. et al. (2020). Double the capacity of manganese spinel for lithium-ion storage by suppression of cooperative Jahn–teller distortion. *Advanced Energy Materials* 10 (34): 2000363.

41 Yang, S., Yan, P., Bao, W. et al. (2023). Surface magnesium substitution at spinel lithium manganate 8a tetrahedral sites for suppressed manganese dissolution and enhanced cycle stability. *ACS Energy Letters* 8: 4278–4286.

42 Chen, C., Feng, J., Li, J. et al. (2022). Functional fiber materials to smart fiber devices. *Chemical Reviews* 123: 613–662.

43 Blasse, G. (1966). Ferromagnetism and ferrimagnetism of oxygen spinels containing tetravalent manganese. *Journal of Physics and Chemistry of Solids.* 27: 383–389.

44 Lee, S., Su, L., Mesnier, A. et al. (2023). Cracking vs surface reactivity in high-nickel cathodes for lithium-ion batteries. *Joule* 7: 2430–2444.

45 Thackeray, M.M. and Amine, K. (2021). Layered Li–Ni–Mn–Co oxide cathodes. *Nature Energy* 6: 933–933.

46 Dopilka, A., Larson, J.M., Cha, H., and Kostecki, R. (2024). Synchrotron near-field infrared nanospectroscopy and nanoimaging of lithium fluoride in solid electrolyte interphases in Li-ion battery anodes. *ACS Nano* 18 (23): 15270–15283.

47 Khan, M., Yan, S., Ali, M. et al. (2024). Innovative solutions for high-performance silicon anodes in lithium-ion batteries: overcoming challenges and real-world applications. *Nano-Micro Letters* 16 (1): 179.

48 Feng, Y., Zhou, L., Ma, H. et al. (2022). Challenges and advances in wide-temperature rechargeable lithium batteries. *Energy & Environmental Science* 15 (5): 1711.

49 Shi, Q.T., Zhou, J.H., Ullah, S. et al. (2021). A review of recent developments in Si/C composite materials for Li-ion batteries. *Energy Storage Materials.* 34: 735–754.

50 Schomburg, F., Heidrich, B., Wennemar, S. et al. (2024). Lithium-ion battery cell formation: status and future directions towards a knowledge-based process design. *Energy & Environmental Science* 17: 2686–2733.

51 Dai, F. and Cai, M. (2022). Best practices in lithium battery cell preparation and evaluation. *Communications Materials* 3: 64.

52 Spielbauer, M., Soellner, J., Berg, P. et al. (2022). Experimental investigation of the impact of mechanical deformation on aging, safety and electrical behavior of 18650 lithium-ion battery cells. *Journal of Energy Storage* 55: 105564.

53 Shen, K., Sun, J., Zheng, Y.J. et al. (2022). A comprehensive analysis and experimental investigation for the thermal management of cell-to-pack battery system. *Applied Thermal Engineering* 211: 118422.

54 Dasari, S.M., Srivastav, P., Shaw, R. et al. (2013). Optimization of cell to module conversion loss by reducing the resistive losses. *Renewable Energy* 50: 82–85.

55 Wang, H.B., Wang, S.Y., Feng, X.N. et al. (2021). An experimental study on the thermal characteristics of the cell-to-pack system. *Energy.* 227: 120338.

56 Man, Q.Y., An, Y.L., Liu, C.K. et al. (2023). Interfacial design of silicon/carbon anodes for rechargeable batteries: a review. *Journal of Energy Chemistry* 76: 576–600.

57 Ge, M.Z., Cao, C.Y., Biesold, G.M. et al. (2021). Recent advances in silicon-based electrodes: from fundamental research toward practical applications. *Advanced Materials* 33 (16).

58 Jin, C.Y., Sun, Y.D., Yao, J. et al. (2022). No thermal runaway propagation optimization design of battery arrangement for cell-to-chassis technology. *ETransportation* 14: 100199.

59 Yao, F., Guenes, F., Huy Quang, T. et al. (2012). Diffusion mechanism of lithium ion through basal plane of layered graphene. *Journal of the American Chemical Society* 134 (20): 8646–8654.

60 Wang, M.S., Wang, G.L., Wang, S. et al. (2019). In situ catalytic growth 3D multi-layers graphene sheets coated nano-silicon anode for high performance lithium-ion batteries. *Chemical Engineering Journal* 356: 895–903.

61 Stevens, D.A. and Dahn, J.R. (2000). High capacity anode materials for rechargeable sodium-ion batteries. *Journal of the Electrochemical Society* 147 (4): 1271.

62 Stevens, D.A. and Dahn, J.R. (2000). An in situ small-angle X-ray scattering study of sodium insertion into a nanoporous carbon anode material within an operating electrochemical cell. *Journal of the Electrochemical Society* 147 (12): 4428.

63 Schomburg, F., Heidrich, B., Wennermar, S. et al. (2024). Lithium-ion battery cell formation: status and future directions towards a knowledge-based process design. *Energy & Environmental Science* 17 (8): 2686–2733.

64 Bai, P., He, Y., Zou, X. et al. (2018). Elucidation of the sodium-storage mechanism in hard carbons. *Advanced Energy Materials* 8 (15): 1703217.

65 Wang, D., Zhou, J., Li, Z. et al. (2019). Uniformly expanded interlayer distance to enhance the rate performance of soft carbon for lithium-ion batteries. *Ionics* 25 (4): 1531–1539.

66 Sun, L., Liu, Y.X., Wu, J. et al. (2022). A review on recent advances for boosting initial coulombic efficiency of silicon anodic lithium ion batteries. *Small* 18 (5): 2102894.

67 Zhang, M., Liang, N., Hao, D. et al. (2023). Recent advances of SiO_x-based anodes for sustainable lithium-ion batteries. *Nano Research Energy* 2: e9120077.

68 Xu, K. (2021). Li-ion battery electrolytes. *Nature Energy* 6: 763.

69 Ye, C., Tu, W., Yin, L. et al. (2018). Converting detrimental HF in electrolytes into a highly fluorinated interphase on cathodes. *Journal of Materials Chemistry A* 6 (36): 17642.

70 Xu, K. (2004). Nonaqueous liquid electrolytes for lithium-based rechargeable batteries. *Chemical Review* 104 (10): 4303–4418.

71 Zhang, Y., Lu, Y., Jin, J. et al. (2024). Electrolyte design for lithium-ion batteries for extreme temperature applications. *Advanced Materials* 36 (13): 2308484.
72 Liu, Y.K., Zhao, C.Z., Zhang, X.Q. et al. (2023). Research progresses of liquid electrolytes in lithium-ion batteries. *Small* 19: 2205315.
73 Zhu, Y.X., Ge, M.Y., Ma, F.C. et al. (2024). Multifunctional electrolyte additives for better metal batteries. *Advanced Functional Materials* 34: 2301964.
74 Zou, F. and Manthiram, A. (2020). A review of the design of advanced binders for high-performance batteries. *Advanced Energy Materials* 10 (45): 2002508.
75 Chen, H., Ling, M., and Hencz, L. (2018). Exploring chemical, mechanical, and electrical functionalities of binders for advanced energy-storage devices. *Chemical Reviews* 118 (18): 8936–8982.
76 Dou, W., Zheng, M., and Zhang, W. (2023). Review on the binders for sustainable high-energy-density lithium ion batteries: status, solutions, and prospects. *Advanced Functional Materials* 33 (45): 2305161.
77 Lux, S.F., Schappacher, F., and Balducci, A. (2010). Low cost, environmentally benign binders for lithium-ion batteries. *Journal of the Electrochemical Society* 157 (3): A320.
78 Shi, Y., Zhou, X., and Yu, G. (2017). Material and structural design of novel binder systems for high-energy, high-power lithium-ion batteries. *Accounts of Chemical Research* 50 (11): 2642–2652.
79 Fransson, L., Eriksson, T., and Edström, K. (2001). Influence of carbon black and binder on Li-ion batteries. *Journal of Power Sources* 101 (1): 1–9.